Published in final edited form as:
Cancer Res. 2010 November 15; 70(22): 9041–9052. doi:10.1158/0008-5472.CAN-10-1369.

A THERAPEUTIC OX40 AGONIST DYNAMICALLY ALTERS DENDRITIC, ENDOTHELIAL AND T CELL SUBSETS WITHIN THE ESTABLISHED TUMOR MICROENVIRONMENT

Angela D. Pardee[1], **Dustin McCurry**[1], **Sean Alber**[2], **Peisheng Hu**[3], **Alan L. Epstein**[3], and **Walter J. Storkus**[1,4,5]

[1]Department of Immunology, University of Pittsburgh School of Medicine, Pittsburgh, PA 15213

[2]Department of Cell Biology and Physiology, University of Pittsburgh School of Medicine, Pittsburgh, PA 15213

[3]Department of Pathology, Keck School of Medicine, University of Southern California, Los Angeles, CA 90033

[4]Department of Dermatology, University of Pittsburgh School of Medicine, Pittsburgh, PA 15213

[5]University of Pittsburgh Cancer Institute, Pittsburgh, PA 15213

Abstract

Little preclinical modeling currently exists to support the use of OX40 agonists as therapeutic agents in the setting of advanced cancers, as well as, the mechanisms through which therapeutic efficacy is achieved. We demonstrate that treatment of mice bearing well-established day 17 sarcomas with a novel OX40 ligand-Fc fusion protein (OX40L-Fc) resulted in tumor regression or dormancy in the majority of treated animals. Unexpectedly, dendritic cells (DC) in the progressive tumor microenvironment (TME) acquire OX40 expression and bind fluorescently-labeled OX40L-Fc. Furthermore, longitudinal analyses revealed that DC become enriched in the tumor-draining lymph node (TDLN) of both wild-type and $Rag^{-/-}$ mice within three days after OX40L-Fc treatment. By day 7 after treatment, a significant expansion of $CXCR3^{+}$ T effector cells was noted in the TDLN, and by day 10 post-treatment, Type-1 polarized T cells exhibiting a re-activated memory phenotype had accumulated in the tumors. High levels of CXCL9 (a CXCR3 ligand) and enhanced expression of VCAM-1 by vascular endothelial cells (VEC) were observed in the TME early after treatment with OX40L-Fc. Notably, these vascular alterations were maintained in $Rag^{-/-}$ mice, indicating that the OX40L-Fc-mediated activation of both DC and VEC occur in a T cell-independent manner. Collectively, these findings support a paradigm in which the stimulation of DC, T cells and the tumor vasculature by an OX40 agonist dynamically orchestrates the activation, expansion and recruitment of therapeutic T cells into established tumors.

Keywords

OX40; T lymphocytes; Dendritic Cells; Vascular Endothelial Cells; Sarcoma

Correspondence to: Walter J. Storkus, Ph.D., Professor of Dermatology and Immunology, University of Pittsburgh School of Medicine, W1041.2 BST, 200 Lothrop Street, Pittsburgh, PA 15213, Tel: 412-648-9981, FAX: 412-383-5857; storkuswj@upmc.edu.

INTRODUCTION

As tumors develop and progress, a number of regulatory mechanisms are responsible for maintaining immune tolerance in the tumor microenvironment (TME). Poor tumor homing and penetration of T effector cells, a consequence of aberrant vasculature and limited chemokine and adhesion molecule expression in the TME (1,2), is one major barrier to anti-tumor immunity (3). Furthermore, tumor-specific T cells that effectively infiltrate tumors may be rendered inactive by soluble factors and inhibitory signals associated with tumor cells and through the negative impact of both myeloid- and lymphoid-derived suppressor cells (4,5). While systemic immunity may be affected to a variable degree, immune suppression is typically most profound within the TME, with tumor-infiltrating lymphocytes (TIL) exhibiting severe deficiencies in $CD8^+$ T cell-mediated cytotoxic function (6). In murine tumor models, TIL dysfunction becomes pronounced only at later stages of solid tumor growth, at which point a mature tumor stroma comprised of both bone marrow- and non-bone marrow-derived cells has been established (7,8).

Given the perceived importance of T cell-mediated immunity underlying effective immunotherapy (9) and better clinical outcome (3), substantial emphasis has recently been placed on the development of treatment modalities that are capable of restoring T cell function and enhancing tumor penetration in the tumor-bearing host. In particular, immune-stimulating agents that target the costimulatory TNF receptor (TNFR) family member OX40, have demonstrated anti-tumor efficacy in pre-clinical models (10). Costimulatory members of the TNFR family are up-regulated shortly after TCR engagement on naïve and antigen-experienced cells, where they serve as key modulators of cell activation, survival, and differentiation (11,12). OX40 is expressed by activated T effector cells and OX40-mediated signals provided during priming regulate $CD4^+$ and $CD8^+$ T cell activation and clonal expansion *in vivo* (13-15). Furthermore, anergic or hypo-responsive $OX40^+$ T cells may be re-activated by OX40 agonists (16). OX40 is also constitutively expressed by $CD4^+Foxp3^+$ regulatory T cells (Treg) (17). Indeed, recent studies have demonstrated that agonist signaling through OX40 inhibits the suppressor function of natural $Foxp3^+$ Treg (18), prevents the induction of Treg from $CD4^+$ T effector cells (19), and confers resistance to effector cells against Treg-mediated inhibition (13).

To characterize the molecular, cellular, and treatment-associated consequences of OX40 engagement in the setting of well-established tumors, a novel agonistic reagent directed against murine OX40 (OX40 ligand-Fc fusion protein; OX40L-Fc) was recently constructed and characterized *in vitro* (20). We observed that the progressive growth of well-established day 17 sarcomas was inhibited by a short course of OX40L-Fc therapy, with complete tumor regression or extended disease stabilization (i.e. tumor dormancy) observed in the majority of treated animals. Comparable findings were obtained in both the MCA205 ($H\text{-}2^b$) and CMS4 ($H\text{-}2^d$) sarcoma models. We noted that i.p. injection of OX40L-Fc induced significant expansion of T effector cells in the TDLN, resulting in the accumulation of activated, Type-1 polarized T cells in the TME within 10 days of initiating OX40L-Fc therapy. Moreover, our therapy appeared to dynamically affect DC and vascular endothelial cells (VEC) in both wild-type and $Rag^{-/-}$ mice bearing well-established tumors. The extensive molecular and cellular alterations observed in this model strongly support the translation of OX40 agonists into human clinical trials, either as single agents or in the context of combinational immunotherapy (21).

MATERIALS AND METHODS

Mice

Six to ten week old female C57BL/6 (H-2^b), B6.129S7-Rag1^{tm1Mom} (Rag$^{-/-}$; H-2^b) and BALB/cJ (H-2^d) mice were purchased from The Jackson Laboratory and maintained in the pathogen-free animal facility in the Biomedical Sciences Tower at the University of Pittsburgh. All animal work was done in accordance with a protocol approved by the Institutional Animal Care and Use Committee.

Tumor Establishment

The MCA205 (H-2^b) sarcoma cell line was purchased from the American Type Culture Collection (ATCC). The CMS4 (H-2^d) sarcoma has been described in detail previously (22). Cell lines were cultured in complete media (CM; RPMI-1640 supplemented with 100 U/ml penicillin, 100 μg/ml streptomycin, 10 mM L-glutamine and 10% heat-inactivated fetal bovine serum (all reagents from Life Technologies) in a humidified incubator at 37° C and 5% CO_2. All cell lines were negative for known mouse pathogens. Tumors were established by injection of 5×10^5 tumor cells s.c. into the right flanks of syngeneic mice, with tumor size assessed every 3 to 4 days and recorded in mm^2. Mice were sacrificed when tumors became ulcerated or reached a maximum size of 400 mm^2.

Costimulatory Therapy

Tumor-bearing mice were injected i.p. with 100 μg of OX40L-Fc or rat IgG isotype control antibody (Sigma-Aldrich) in a total volume of 100 μl PBS on days 17 and 20 post-tumor inoculation when tumors were approximately 30-50 mm^2 in size. The mOX40L-Fc fusion protein has been previously described (20).

Isolation of Tumor, LN and Spleen cells

Single cell suspensions were obtained from TDLN as previously described (22). For TIL, tumors were enzymatically digested with 0.1% w/v collagenase, 1% w/v hyaluronidase, and 0.1% w/v DNase (all from Sigma), with lymphocytes isolated as buoyant cells after discontinuous density centrifugation as previously described (23).

In Vitro Stimulation (IVS) of T cells

Bulk TIL (n = 1 per group) were restimulated *in vitro* with irradiated (100 Gy) MCA205 cells for 5 days at a T cell-to-tumor ratio of 10:1 in CM with 20 U/ml recombinant human IL-2. Recovered T cells were then cultured in media alone (to determine background cytokine levels) or with 5μg/ml anti-CD3 (BioLegend) for 72 hours. Cell-free supernatants were then harvested and assessed for levels of mIFN-γ using a specific OptEIA ELISA set (BD Biosciences) according to the manufacturer's instructions with a lower limit of detection of 32.5 pg/ml. Data are reported as the mean ± SD of duplicate determinations.

RT-PCR

Total RNA was isolated from TIL on days 3, 7, and 10 after the initial treatment (day 17 post-tumor inoculation), as indicated, using RNeasy Micro kit (Qiagen), according to the manufacturer's instructions. For semi-quantitative RT-PCR, TIL were cultured with 5 μg/ml anti-CD3 (BioLegend) for 24 hours, followed by RNA isolation and cDNA preparation using random hexamer primers (Applied Biosciences). PCR was performed using the primer pairs listed in Table S1. Cycling times and temperature were as follows: initial denaturation at 94°C for 2 min (1 cycle), denaturation at 94°C for 30 s, annealing at 60-65°C for 30 s and elongation at 72°C for 1 min (35-40 cycles), final extension at 72°C for 5 min (1 cycle). Following gel electrophoresis, PCR products were imaged and band density quantified using

LabWorks Software (PerkinElmer). For quantitative RT-PCR, reverse transcription and PCR amplification was performed by the University of Pittsburgh's Genomics and Proteomics Core Laboratories (a shared resource). For quantitative analysis of T-bet, IFN-γ, and control β-actin, previously published primer pairs were used (24), and cDNA was amplified using SYBR® Green PCR Master Mix (Applied Biosystems). For quantitative analysis of Foxp3, IL-10, and control β-actin, RT^2 qPCR Primer Assays (SABiosciences) were used and cDNA was amplified using RT^2 SYBR Green qPCR Master Mix (SABiosciences). For each sample, the cycle threshold (Ct) values for β-actin gene were determined for normalization purposes and the ΔCt between β-actin and T-bet, Foxp3, IFN-γ and IL-10 were calculated. ΔΔCt were calculated to isotype treatment samples. Relative RNA expression for each gene is depicted as $2^{\Delta\Delta Ct}$.

Confocal Immunofluorescence Staining and Imaging

Tumor tissue was processed and sectioned as previously reported (22), followed by immunofluorescence staining and confocal microscopy. The following primary antibodies were used for staining sections: rat anti-mouse CD31 (BD Biosciences), goat anti-mouse OX40 (Santa Cruz Biotechnology), rat anti-mouse OX40 (eBioscience), hamster anti-mouse CD11c (BD Biosciences), rat anti-mouse VCAM-1 (Santa Cruz Biotechnology), and goat anti-mouse CXCL9 (R&D Systems). The following secondary antibodies were used: donkey anti-rat Alexa Fluor 488 (Molecular Probes), donkey anti-goat Cy3 (Jackson ImmunoResearch), donkey anti-hamster Alexa Fluor 488 (Molecular Probes), donkey anti-rat Cy3 (Jackson ImmunoResearch), goat anti-rat Fab1 fragment Cy3 (Jackson ImmunoResearch), and goat anti-rat Alexa Fluor 488 (Molecular Probes). All sections were briefly incubated with DAPI (Sigma) and then mounted. Images were acquired using an Olympus Fluoview 1000 confocal microscope (Olympus). Isotype control and specific antibody images were taken using the same level of exposure on the channel settings.

Flow Cytometry

Before all stainings, cells were Fc-blocked with anti-CD16/CD32 (BD). Single-cell suspensions were stained using the following antibodies: PerCP- and PE-conjugated CD4 and CD8, PE-conjugated Gr-1, FITC-conjugated CD80 and CD25, and PerCP-Cy5.5-conjugated Ki67 (all BD), FITC-conjugated CD27, Class II and F4/80, PE-conjugated CCR7 and OX40, and APC-conjugated CD11c, CD44, CXCR3, and CD11b (all eBioscience) or appropriate-matched, fluorochrome-labeled isotype control mAb. For Foxp3 intracellular staining, $CD4^+$ T cells were surface stained as described above and then further processed using an APC anti-mouse/rat Foxp3 Staining kit (eBioscience) according to the manufacturer's instructions. FITC-conjugation of OX40L-Fc was performed using a FITC protein labeling kit (Molecular Probes). Cells were analyzed using an LSR II flow cytometer (Beckman Coulter), with corollary data assessed using FlowJo software (version 7.6.1; Tree Star, Inc.).

Statistical Analysis

All comparisons of inter-group means were performed using a two-tailed Student's *t* test, with P values < 0.05 considered significant.

RESULTS

OX40L-Fc treatment elicits potent anti-tumor activity against well-established tumors

A novel OX40 agonist, consisting of mOX40L linked to the C-terminus of the Fc fragment of immunoglobulin, was recently constructed and shown to be curative in early day 5 ($H\text{-}2^d$) Colon 26 and RENCA tumor models (20). In contrast, an agonist anti-OX40 (OX86) mAb

was only able to extend median survival by approximately 2 weeks in these models. To determine whether OX40L-Fc would be efficacious in a more established and potentially clinically-relevant disease model, we treated H-2^b mice bearing day 17 MCA205 sarcomas via i.p. injection of 100 μg of OX40L-Fc or control rat IgG. A second identical dose was provided three days later. Tumors in all control-treated mice grew progressively and exhibited a rapid expansion in size around day 30 post-inoculation, necessitating euthanasia by day 40 (Fig. 1A). In contrast, OX40L-Fc-treated mice exhibited reduced, stabilized tumor size by day 27 that was durable through day 40. Although OX40L-Fc treatment resulted in the long-term survival of only 13% of treated animals (Fig. 1B), 50% of this cohort exhibited small (~20-40 mm^2) lesions that remained "dormant" for more than 6 weeks, before eventually progressing. Growth of representative tumors exhibiting dormancy in OX40L-Fc-treated mice is shown in Fig. 1C.

Similar therapeutic benefits were observed in the CMS4 (H-2^d) sarcoma model, where over 80% of animals rejected their tumors after OX40L-Fc treatment on days 17 and 20 (Fig. S1). Despite the superior efficacy observed for OX40L-Fc in the CMS4 model, all remaining data were collected in the MCA205 tumor model due to the tendency of progressor CMS4 tumors to ulcerate, necessitating pre-mature euthanasia per IACUC regulations.

T cell and DC expression of OX40 is elevated in the progressor TME

To identify the *in situ* cellular targets of OX40L-Fc-based therapy, we next assessed OX40 expression on T cell subsets within the TDLN and the TME of untreated MCA205 tumor-bearing mice between days 17 and 20 post-tumor inoculation. While OX40 was barely detectable on $CD4^+Foxp3^-$ and $CD8^+$ T cells in the TDLN, approximately 50% of $CD4^+Foxp3^+$ T cells expressed OX40 (Fig. 2A), consistent with previous reports indicating that OX40 expression is restricted to the regulatory subset of resting T cells in peripheral tissues (13). Conversely, OX40 expression was up-regulated on all T cell subsets in the untreated TME, including a median of over 20% of $CD8^+$ T cells and over 60% of $CD4^+Foxp3^-$ T cells.

Because NK and NKT cells can express OX40 under certain conditions (25,26), we hypothesized that non-T cell subsets may also represent targets for interaction with OX40L-Fc in the progressor TME. Indeed, OX40 expression was highly up-regulated on $CD11c^+CD11b^+ClassII^{hi}$ tumor-infiltrating DC (TIDC) when compared to TDLN-localized DC (median of 37.6% vs. 2.3% $OX40^+$, respectively; Fig. 2B). OX40 was also detected on TIDC via confocal immunofluorescence microscopy (Fig. 2C). Furthermore, FITC-labeled OX40L-Fc was found to bind to TIDC, but not to TDLN-localized DC (Fig. 2D). These data suggest that although $CD4^+Foxp3^+$ T cells may represent the exclusive expressors of OX40 in the periphery, $CD4^+Foxp3^-$ and $CD8^+$ T effector cells, as well as DC, contain substantial $OX40^+$ populations in the TME, making each of these cell types plausible targets of OX40L-Fc-based therapy.

T cell-independent enrichment of mature DC expressing the LN-homing receptor CCR7 in the TDLN shortly after treatment with OX40L-Fc

Given the observed high levels of OX40 expressed by TIDC in untreated tumor-bearing mice, we next evaluated how DC populations were altered in response to OX40L-Fc treatment. By day 3 after the first OX40L-Fc treatment, TIDC expression of the costimulatory molecules CD80 and CD86 was augmented (data not shown), and a concordant increase in $CD11c^+CD11b^+$ DC within the TDLN was observed when compared to isotype mAb-treated control mice (Fig. 3A). These TDLN DC populations expressed elevated levels of CD80 and the lymph node-homing chemokine receptor CCR7 when compared to TDLN isolated from isotype mAb-treated control animals (Fig. S2). Moreover,

enrichment of DC upon OX40L-Fc treatment was similarly observed in the TDLN of $Rag^{-/-}$ mice bearing established MCA205 tumors (Fig. 3B). These data are consistent with the T cell-independent activation/maturation of $OX40^+$ TIDC to become competent for trafficking to the TDLN within the initial 3 days of OX40L-Fc-based therapy. Longitudinal analysis suggests that treatment-induced migration of TIDC to the TDLN persists through day 7 of the therapy period, with a return to control conditions by day 10 (data not shown). Such trafficking of activated DC would be anticipated to sponsor the cross-priming of anti-tumor T cell responses in the TDLN. We observed no substantial alterations, however, in DC frequency or phenotype in non-TDLN (data not shown).

OX40L-Fc treatment promotes the expansion of TDLN T cells expressing the tissue-homing Type-1 chemokine receptor CXCR3

To assess alterations in the TDLN T cell compartment following OX40L-Fc treatment and TIDC trafficking to the TDLN, we harvested TDLN from mice on days 3, 7, and 10 after initiating treatment and determined absolute numbers of $CD4^+Foxp3^-$ and $CD8^+$ T effector cells. Time-dependent increases in both T cell sub-populations were noted as a consequence of OX40L-Fc treatment, with numbers of TDLN T cells peaking at day 7 post-treatment (Fig. 3C). Indeed, 7 days after initiating OX40L-Fc treatment, highly significant up-regulation in expression of the proliferation marker Ki67 was observed for both $CD4^+$ and $CD8^+$ T cell subsets within the TDLN ($P < 0.01$; Fig. 3D). Although these T cells did not exhibit any alterations in activation marker expression (CD25 and CD69; data not shown), both $CD4^+$ and $CD8^+$ T cells expanded from OX40L-Fc-treated versus control mAb-treated mice were enriched in the $CD44^{hi}$ phenotype at day 7 post-treatment (Fig. S3A), supporting the ability of OX40L-Fc therapy to preferentially stimulate memory T cells.

It has recently been demonstrated that Type-1 polarized $CD8^+$ T cells are effectively recruited to tumor sites via CXCR3-mediated chemotaxis in response to the CXCL9-11 chemokines produced within the TME (27). To determine whether TDLN T cells in OX40L-Fc-treated animals are differentially competent to migrate to the TME based on this index, we assessed $CD4^+$ and $CD8^+$ T cells for their expression of CXCR3 7 days after the initiation of therapy. As shown in Fig. S3B, we found that the $CXCR3^+$ sub-population of $CD4^+$ and $CD8^+$ T cells was increased after OX40L-Fc versus control mAb treatment. These data suggest that OX40 agonist therapy not only stimulates expansion of TDLN T cells, but also licenses these cells for trafficking to peripheral tissue sites in which CXCR3 ligands are expressed, such as the TME.

Tumors become enriched in T effector cells by day 10 following OX40L-Fc treatment

Based on our observation that maximal numbers of $CXCR3^+$ TDLN T cells occurred by day 7 after OX40L-Fc treatment, we hypothesized that these transport-competent T cells might then infiltrate the TME shortly thereafter. Although increased frequencies of $CD4^+Foxp3^-$ and $CD8^+$ T effector cells were detected in the TME throughout the observation period, a highly significant increase versus control mAb-treated animals was noted for $CD4^+Foxp3^-$ TIL at days 7 and 10 post-treatment and $CD8^+$ TIL at day 10 post-treatment ($P < 0.01$; Fig. 4A). The change in percentages of T effector cells correlated with increases in the number of $CD4^+Foxp3^-$ and $CD8^+$ TIL per gram of tumor tissue (Fig. S4). In order to distinguish between the recruitment of T effector cells and *in situ* T cell expansion within the TME, TIL were analyzed for their expression of Ki67. While Ki67 expression was up-regulated by T cells in the TDLN of OX40LFc-treated mice (Fig. 3D), expression of this marker on TIL was not substantially altered (Fig. 4B), suggesting that T effector cell accumulation in the TME of treated mice is most likely attributed to the enhanced recruitment of these cells, rather than to their expansion within tumor lesions.

Despite an elevated frequency of $CD4^+Foxp3^+$ T cells being consistently identified in the TDLN of OX40L-Fc-treated mice (Fig. S5A), the frequency of these cells in the TME was reduced as early as day 3 post-treatment and this level remained low throughout the observation period (Fig. S5B), consistent with a recent report (28). Additionally, a decrease in cells exhibiting a myeloid-derived suppressor cell phenotype ($CD11b^+Gr\text{-}1^+$) was observed in the TME, along with a coordinate increase in $F4/80^+$ mature monocytes/macrophages between days 7 and 10 post-treatment (Fig. S6).

Tumor infiltrating T cells exhibit a re-activated memory phenotype and are Type-1 polarized

An analysis of the phenotype of TIL on day 10 after OX40L-Fc treatment, at which time T effector cell frequencies in the TME peaked, suggested no differential expression of CD25 or CD69 versus the control mAb-treated cohort (data not shown). However, the frequency of $CD4^+$ and $CD8^+$ TIL expressing high levels of CD44 ($CD44^{hi}$, antigen-experienced) and low levels of CD27 ($CD27^{low}$, recently-activated) was enriched at this time point (Figs. 4C and S7). These phenotypic analyses are consistent with a model in which OX40L-Fc-stimulated T cells are expanded in the TDLN by day 7 post-treatment and subsequently infiltrate the TME by day 10 post-treatment.

Because effective cancer immunotherapies have been largely associated with a state of Type-1 T cell polarization and an increased T effector cell-to-Treg ratio (29,30), we next examined the polarization status of freshly-isolated TIL on days 3-10 following OX40L-Fc- versus control mAb-treatment. Using quantitative RT-PCR, factors associated with Type-1 T cell activity (i.e. T-bet and IFN-γ) and those associated with regulatory T cell activity (i.e. Foxp3 and IL-10) were assessed for their relative levels of expression. Although minimal alterations were observed in the expression of any of these four transcripts on days 3 and 7 post-treatment, by day 10 post-treatment, at a time when increased frequencies of TIL were observed, transcript levels for all 4 gene products were dramatically enhanced in the OX40L-Fc treatment group. (Fig. 5A, **upper panels**). This is consistent with a recent report by Ruby and colleagues, who propose that while all T cell lineages are responsive to OX40 stimulation, the plasticity of the response is dependent on the local cytokine milieu (31). By considering the “balance” of polarized T cell responses based on a ratio of the effector-to-regulatory gene transcripts, however, we noted that OX40L-Fc treatment skews the balance in favor of Type-1 T cell immunity at all time points analyzed (Fig. 5A, **lower panels**). Similar alterations in these transcript ratios were observed in anti-CD3-stimulated TIL (Fig. 5B). This suggests that although OX40 signaling may not be a polarizing event *per se*, a cytokine milieu appropriate for the preferential expansion of Type-1 versus regulatory-type immunity exists within the OX40L-Fc-treated TME.

To ensure that alterations in IFN-γ RNA expression correlated with alterations at the protein level, TIL were isolated on days 3-10 post-treatment and stimulated *in vitro* prior to analysis of IFN-γ secretion levels by ELISA. Interestingly, TIL production of IFN-γ was not elevated, and perhaps even slightly reduced on day 3 after treatment with OX40L-Fc versus isotype mAb (Fig. 5C). In contrast, TIL isolated 7 and 10 days after initiating OX40L-Fc-based therapy produced significantly higher levels of IFN-γ protein versus TIL harvested from control mAb-treated mice at these same time points. Moreover, when comparing the effector-to-regulatory balance at the cellular level within the TME, significant increases were observed in both the $CD4^+Foxp3^-$ and $CD8^+$ T effector versus Treg ratios at days 7 and 10 post-treatment ($P < 0.01$; Fig. 5D).

OX40L-Fc treatment renders the TME permissive to Type-1 T cell infiltration via modulation of the tumor vasculature

In parallel with an increased fraction of $CXCR3^+$ T cells in the TDLN of OX40L-Fc-treated mice, CXCL9 (a CXCR3 ligand) was dramatically up-regulated in the TME between days 7 and 10 post-treatment (Fig. 6A, **left panels**), indicating that OX40L-Fc therapy redundantly promotes TIL trafficking by augmenting chemokine signals in both the periphery and the TME. We have also recently reported that effective recruitment of adoptively-transferred Type-1 polarized $CD8^+$ T cells into the TME requires tumor-associated VEC expression of VCAM-1 (32). Confocal immunofluorescence microscopy revealed that tumor-associated $CD31^+$ VEC rapidly up-regulate (i.e. by day 3) and maintain VCAM-1 expression through day 10 as a consequence of treatment with OX40L-Fc (Fig. 6B, **left panels**), suggesting that Type-1 T effector cell recruitment into the TME might be further enhanced by OX40L-Fc via additional, chemokine-independent mechanisms. Importantly, treatment-associated enhancement of VCAM-1 and CXCL9 expression by $CD31^+$ VEC was recapitulated in $Rag^{-/-}$ mice (Fig. 6A and B, **right panels**), suggesting the T cell-independent nature of these changes. In support of a direct effect of OX40L-Fc on VEC within the TME, we detected moderate levels of OX40 expression by a subset of $CD31^+CD11b^-$ VEC in untreated, progressor tumors (Fig. S8). It is also important to note that Fig. 6A data suggest that additional (non-VEC) stromal cells in the TME produce CXCL9 in wild-type, but not $Rag^{-/-}$ mice (most strikingly on day 7 post-treatment with OX40L-Fc). Hence, therapeutic production of CXCL9 in the TME appears to result from both T cell-dependent and T cell-independent processes.

We also observed a pronounced reorganization of the tumor vasculature after OX40L-Fc treatment, consistent with what has previously been described as a more “normalized” phenotype (33). While $CD31^+$ VEC density increased coordinately with disease progression in the tumors of isotype control mAb-treated mice, vessel density in OX40L-Fc-treated tumors was significantly diminished by day 10 post-treatment (Fig. S9A). These alterations in vascular density at day 10 post-treatment additionally correlated with a less tortuous and more organized (i.e. normalized) morphology of OX40L-Fc- versus control mAb-treated tumor vasculature (Fig. S9B), consistent with a phenotype favorable for lymphocyte infiltration.

DISCUSSION

In this report, we describe multifaceted anti-tumor activities associated with a novel mOX40L-Fc fusion protein when applied in the therapeutic setting against well-established $H\text{-}2^b$ and $H\text{-}2^d$ sarcomas. When administered i.p. on days 17 and 20 post-tumor inoculation, OX40L-Fc treatment inhibited tumor growth, resulting in disease stabilization or complete regression in the majority of treated animals.

In the TDLN of mice bearing well-established MCA205 sarcomas, OX40 expression was restricted to $CD4^+Foxp3^+$ T cells, whereas $CD4^+Foxp3^-$ and $CD8^+$ T effector cells, as well as DC and potentially VEC, were observed to be $OX40^+$ in the TME. Expression of OX40 has also been reported to be up-regulated by T cells in primary tumors, but not in the tumor-free lymph nodes of human cancer patients (34). In alternative disease models, T cell up-regulation of OX40 has been observed at sites of inflammation during the onset of experimental autoimmune encephalomyelitis (35), and within the synovial fluid, but not the peripheral blood of patients with rheumatoid arthritis (36). This has been attributed to the influence of inflammatory cytokines, including IL-1 and TNF-α (37,38). Such cytokines could also play a role in up-regulating the expression of OX40 by tumor-localized DC and VEC in our well-established sarcoma models. Furthermore, 4-1BB, an alternate member of the costimulatory TNFR family with structural and functional similarities to OX40, can be

expressed by activated DC and atherosclerotic endothelia under the appropriate conditions (39,40).

Numerous studies have indicated that both $CD4^+$ and $CD8^+$ T effector cells play instrumental roles in anti-tumor immunity stimulated by OX40 agonists *in vivo* (41). Consistent with this notion, we observed significant expansion of $CXCR3^+$ TDLN T effector cells on day 7 after initiating OX40L-Fc-based therapy, followed on day 10 post-treatment by the accumulation of re-activated, Type-1 polarized $CD4^+Foxp3^-$ and $CD8^+$ T cells in the TME. Our data from $Rag^{-/-}$ models also now suggest the T cell-independent nature of OX40L-Fc-mediated events, including: i.) the rapid and sustained production of CXCL9 and expression of VCAM-1 on VEC in established tumors, and ii.) the conversion of $OX40^+$ TIDC into transport-competent APC (deduced from the subsequent enrichment of $CD11c^+CCR7^+$ myeloid DC in the TDLN by day 3 post-treatment). Although a recent study has demonstrated a similar enhancement in DC trafficking to the TDLN upon treatment with OX40 agonist mAb in an early-stage tumor model, this finding was attributed to therapy-mediated suppression of Treg function and to a corollary restoration in the migratory capacity of TIDC (42). Instead, based on the constitutive expression of OX40 by a sub-population of TIDC in the well-established TME and the preservation of DC alterations in $Rag^{-/-}$ mice following OX40L-Fc treatment, these alterations may occur via the direct engagement of OX40 on these cells. To unequivocally demonstrate a direct effect of OX40L-Fc on TIDC, prospective therapeutic models employing chimeric mice in which only DC are genetically deficient in expression of OX40 will be pursued.

The importance of manipulating the tumor vasculature to attract T cells has recently been demonstrated by Quezada and colleagues, who report ICAM and VCAM up-regulation in the TME upon prophylactic Treg cell depletion as well as therapeutic vaccination (Gvax)/anti-CTLA-4 combination treatment (43), indicating that vascular activation may be achieved through several distinct mechanisms. Similar to our data, activation of the tumor vasculature in these models correlated with enhanced T cell infiltration, increased T effector-to-Treg cell ratios and improved therapeutic efficacy. Our data further suggest that therapy-associated induction of chemokines and adhesion molecules that render the TME more permissive to immune cell infiltration can be achieved in the absence of T cells. OX40L-Fc could conceivably mediate vascular activation in the TME of $Rag^{-/-}$ mice via: i.) direct stimulation of a subset of $OX40^+$ VEC, ii.) inflammatory cytokine/chemokine production by $OX40^+$ TIDC, or iii.) the participation of alternate inflammatory (i.e. NK among others) effector cells present in these mice. The initial effects of nonhematopeoietic and/or innate immune cell subsets in therapy-mediated vascular activation, however, are likely to synergize with the effects mediated by T cells in immune competent hosts. In our model, for example, initial secretion of inflammatory cytokines (i.e. TNF-α) by $OX40^+$ TIDC upon OX40L-Fc treatment may induce CXCL9 and VCAM-1 expression in the TME, allowing for the recruitment of Type-1 polarized T effector cells that produce IFN-γ (a potent inducer of CXCL9 and other angiostatic chemokines), resulting in further remodeling of the tumor vasculature and enhanced T cell infiltration. Future studies will investigate the validity of this paradigm.

Based on the tumor growth curves of OX40L-Fc- versus control mAb-treated mice, the impact of therapy only becomes apparent by 7-10 days after the initiation of therapy. This is consistent with the infiltration of a highly-reactive $CD27^{low}CD44^{hi}$ $CD8^+$ T effector cell population into the TME. As OX40 signaling has been previously shown to enhance recall responses and to preferentially expand $CD44^{hi}$ memory T cells upon antigen rechallenge (44,45), this may suggest that OX40L-Fc treatment leads to the expansion of a tumor antigen-experienced, rather than naïve, T effector cell population in the TDLN, and subsequent trafficking of these T cells to the TME. Regardless, these infiltrating T cells

appear competent to promote tumor regression or to regulate a state of tumor dormancy (i.e. stable disease) in the majority of OX40L-Fc-treated animals for a period of several weeks prior to the ultimate “escape” of progressor lesions. We are currently investigating whether this late progression event results from the erosion of protective anti-tumor T cell responses, the outgrowth of less-immunogenic tumor cell variants, and/or the reacquisition of aberrant vascular structures in the TME (46). If the former mechanism underlies the ultimate failure of OX40L-Fc to induce complete tumor rejection, we would anticipate the enhanced benefits of extending the number of treatment cycles involving OX40 agonists.

Overall, the therapeutic benefits demonstrated for OX40L-Fc in our well-established sarcoma models strongly supports the continued translation of OX40 agonists, particularly those based on a recombinant form of OX40L, into human clinical trials. Moving forward, it will be important to better delineate how the various $OX40^+$ target cell populations within the TME (and elsewhere) are impacted by OX40-mediated signals in order to select potential co-therapeutic agents and to define a strategically-rational schedule for the administration of each modality to yield maximal treatment benefit.

Supplementary Material

Refer to Web version on PubMed Central for supplementary material.

Acknowledgments

The authors wish to thank Drs. J. Taylor, L. Butterfield, N. Giannoukakis, M. Shurin, A. Thomson, and S. Watkins for their constructive comments used in developing this manuscript. The authors also wish to thank Deborah Hollingshead at the University of Pittsburgh's Genomics and Proteomics Core Laboratories for assistance with qRT-PCR and data analysis.

This work was supported by NIH grants 5R01 CA114071-05 (to W.J.S.) and 5T32 CA082084-09 (to A.D.P.). The authors have no conflicting financial interests.

REFERENCES CITED

1. Hamzah J, Jugold M, Kiessling F, et al. Vascular normalization in Rgs5-deficient tumours promotes immune destruction. Nature. 2008; 453:410–4. [PubMed: 18418378]
2. Ganss R, Ryschich E, Klar E, Arnold B, Hammerling GJ. Combination of T-cell therapy and trigger of inflammation induces remodeling of the vasculature and tumor eradication. Cancer Res. 2002; 62:1462–70. [PubMed: 11888921]
3. Galon J, Costes A, Sanchez-Cabo F, et al. Type, density, and location of immune cells within human colorectal tumors predict clinical outcome. Science. 2006; 313:1960–4. [PubMed: 17008531]
4. Gajewski TF, Meng Y, Blank C, et al. Immune resistance orchestrated by the tumor microenvironment. Immunol Rev. 2006; 213:131–45. [PubMed: 16972901]
5. Zou W. Immunosuppressive networks in the tumour environment and their therapeutic relevance. Nat Rev Cancer. 2005; 5:263–74. [PubMed: 15776005]
6. Zippelius A, Batard P, Rubio-Godoy V, et al. Effector function of human tumor-specific CD8 T cells in melanoma lesions: a state of local functional tolerance. Cancer Res. 2004; 64:2865–73. [PubMed: 15087405]
7. Yu P, Lee Y, Liu W, et al. Intratumor depletion of $CD4^+$ cells unmasks tumor immunogenicity leading to the rejection of late-stage tumors. J Exp Med. 2005; 201:779–91. [PubMed: 15753211]
8. Yu P, Rowley DA, Fu YX, Schreiber H. The role of stroma in immune recognition and destruction of well-established solid tumors. Curr Opin Immunol. 2006; 18:226–31. [PubMed: 16459066]
9. Wang E, Miller LD, Ohnmacht GA, et al. Prospective molecular profiling of melanoma metastases suggests classifiers of immune responsiveness. Cancer Res. 2002; 62:3581–6. [PubMed: 12097256]
10. Melero I, Hervas-Stubbs S, Glennie M, Pardoll DM, Chen L. Immunostimulatory monoclonal antibodies for cancer therapy. Nat Rev Cancer. 2007; 7:95–106. [PubMed: 17251916]

11. Sabbagh L, Snell LM, Watts TH. TNF family ligands define niches for T cell memory. Trends Immunol. 2007; 28:333–9. [PubMed: 17597006]
12. Watts TH. TNF/TNFR family members in costimulation of T cell responses. Annu Rev Immunol. 2005; 23:23–68. [PubMed: 15771565]
13. Takeda I, Ine S, Killeen N, et al. Distinct roles for the OX40-OX40 ligand interaction in regulatory and nonregulatory T cells. J Immunol. 2004; 172:3580–9. [PubMed: 15004159]
14. Bansal-Pakala P, Halteman BS, Cheng MH, Croft M. Costimulation of CD8 T cell responses by OX40. J Immunol. 2004; 172:4821–5. [PubMed: 15067059]
15. Gramaglia I, Jember A, Pippig SD, Weinberg AD, Killeen N, Croft M. The OX40 costimulatory receptor determines the development of CD4 memory by regulating primary clonal expansion. J Immunol. 2000; 165:3043–50. [PubMed: 10975814]
16. Bansal-Pakala P, Jember AG, Croft M. Signaling through OX40 (CD134) breaks peripheral T-cell tolerance. Nat Med. 2001; 7:907–12. [PubMed: 11479622]
17. McHugh RS, Whitters MJ, Piccirillo CA, et al. $CD4^+CD25^+$ immunoregulatory T cells: gene expression analysis reveals a functional role for the glucocorticoid-induced TNF receptor. Immunity. 2002; 16:311–23. [PubMed: 11869690]
18. Valzasina B, Guiducci C, Dislich H, Killeen N, Weinberg AD, Colombo MP. Triggering of OX40 (CD134) on $CD4^+CD25^+$ T cells blocks their inhibitory activity: a novel regulatory role for OX40 and its comparison with GITR. Blood. 2005; 105:2845–51. [PubMed: 15591118]
19. So T, Croft M. Cutting edge: OX40 inhibits TGF-β- and antigen-driven conversion of naive CD4 T cells into $CD25^+Foxp3^+$ T cells. J Immunol. 2007; 179:1427–30. [PubMed: 17641007]
20. Sadun RE, Hsu WE, Zhang N, et al. Fc-mOX40L fusion protein produces complete remission and enhanced survival in 2 murine tumor models. J Immunother. 2008; 31:235–45. [PubMed: 18317364]
21. Pardee AD, Wesa AK, Storkus WJ. Integrating costimulatory agonists to optimize immune-based cancer therapies. Immunotherapy. 2009; 1:249–64. [PubMed: 20046961]
22. Berhanu A, Huang J, Alber SM, Watkins SC, Storkus WJ. Combinational FLt3 ligand and granulocyte macrophage colony-stimulating factor treatment promotes enhanced tumor infiltration by dendritic cells and antitumor $CD8^+$ T-cell cross-priming but is ineffective as a therapy. Cancer Res. 2006; 66:4895–903. [PubMed: 16651446]
23. Sasaki K, Pardee AD, Qu Y, et al. IL-4 suppresses very late antigen-4 expression which is required for therapeutic Th1 T-cell trafficking into tumors. J Immunother. 2009; 32:793–802. [PubMed: 19752754]
24. Tayade C, Fang Y, Black GP, AP V Jr. Erlebacher A, Croy BA. Differential transcription of Eomes and T-bet during maturation of mouse uterine natural killer cells. J Leukoc Biol. 2005; 78:1347–55. [PubMed: 16204645]
25. Liu C, Lou Y, Lizee G, et al. Plasmacytoid dendritic cells induce NK cell-dependent, tumor antigen-specific T cell cross-priming and tumor regression in mice. J Clin Invest. 2008; 118:1165–75. [PubMed: 18259609]
26. Zaini J, Andarini S, Tahara M, et al. OX40 ligand expressed by DCs costimulates NKT and CD4+ Th cell antitumor immunity in mice. J Clin Invest. 2007; 117:3330–8. [PubMed: 17975668]
27. Nishimura F, Dusak JE, Eguchi J, et al. Adoptive transfer of type 1 CTL mediates effective anti-central nervous system tumor response: critical roles of IFN-inducible protein-10. Cancer Res. 2006; 66:4478–87. [PubMed: 16618775]
28. Hirschhorn-Cymerman D, Rizzuto GA, Merghoub T, et al. OX40 engagement and chemotherapy combination provides potent antitumor immunity with concomitant regulatory T cell apoptosis. J Exp Med. 2009; 206:1103–16. [PubMed: 19414558]
29. Kemp RA, Ronchese F. Tumor-specific Tc1, but not Tc2, cells deliver protective antitumor immunity. J Immunol. 2001; 167:6497–502. [PubMed: 11714817]
30. Quezada SA, Peggs KS, Curran MA, Allison JP. CTLA4 blockade and GM-CSF combination immunotherapy alters the intratumor balance of effector and regulatory T cells. J Clin Invest. 2006; 116:1935–45. [PubMed: 16778987]

31. Ruby CE, Yates MA, Hirschhorn-Cymerman D, et al. Cutting Edge: OX40 agonists can drive regulatory T cell expansion if the cytokine milieu is right. J Immunol. 2009; 183:4853–7. [PubMed: 19786544]
32. Sasaki K, Zhu X, Vasquez C, et al. Preferential expression of very late antigen-4 on type 1 CTL cells plays a critical role in trafficking into central nervous system tumors. Cancer Res. 2007; 67:6451–8. [PubMed: 17616706]
33. Jain RK. Normalization of tumor vasculature: an emerging concept in antiangiogenic therapy. Science. 2005; 307:58–62. [PubMed: 15637262]
34. Weinberg AD, Rivera MM, Prell R, et al. Engagement of the OX-40 receptor in vivo enhances antitumor immunity. J Immunol. 2000; 164:2160–9. [PubMed: 10657670]
35. Weinberg AD, Bourdette DN, Sullivan TJ, et al. Selective depletion of myelin-reactive T cells with the anti-OX-40 antibody ameliorates autoimmune encephalomyelitis. Nat Med. 1996; 2:183–9. [PubMed: 8574963]
36. Giacomelli R, Passacantando A, Perricone R, et al. T lymphocytes in the synovial fluid of patients with active rheumatoid arthritis display CD134-OX40 surface antigen. Clin Exp Rheumatol. 2001; 19:317–20. [PubMed: 11407087]
37. Horai R, Nakajima A, Habiro K, et al. TNF-α is crucial for the development of autoimmune arthritis in IL-1 receptor antagonist-deficient mice. J Clin Invest. 2004; 114:1603–11. [PubMed: 15578092]
38. Nakae S, Asano M, Horai R, Sakaguchi N, Iwakura Y. IL-1 enhances T cell-dependent antibody production through induction of CD40 ligand and OX40 on T cells. J Immunol. 2001; 167:90–7. [PubMed: 11418636]
39. Olofsson PS, Soderstrom LA, Wagsater D, et al. CD137 is expressed in human atherosclerosis and promotes development of plaque inflammation in hypercholesterolemic mice. Circulation. 2008; 117:1292–301. [PubMed: 18285570]
40. Wilcox RA, Chapoval AI, Gorski KS, et al. Cutting edge: Expression of functional CD137 receptor by dendritic cells. J Immunol. 2002; 168:4262–7. [PubMed: 11970964]
41. Gough MJ, Ruby CE, Redmond WL, Dhungel B, Brown A, Weinberg AD. OX40 agonist therapy enhances CD8 infiltration and decreases immune suppression in the tumor. Cancer Res. 2008; 68:5206–15. [PubMed: 18593921]
42. Piconese S, Valzasina B, Colombo MP. OX40 triggering blocks suppression by regulatory T cells and facilitates tumor rejection. J Exp Med. 2008; 205:825–39. [PubMed: 18362171]
43. Quezada SA, Peggs KS, Simpson TR, Shen Y, Littman DR, Allison JP. Limited tumor infiltration by activated T effector cells restricts the therapeutic activity of regulatory T cell depletion against established melanoma. J Exp Med. 2008; 205:2125–38. [PubMed: 18725522]
44. Ruby CE, Redmond WL, Haley D, Weinberg AD. Anti-OX40 stimulation in vivo enhances $CD8^+$ memory T cell survival and significantly increases recall responses. Eur J Immunol. 2007; 37:157–66. [PubMed: 17183611]
45. Salek-Ardakani S, Song J, Halteman BS, et al. OX40 (CD134) controls memory T helper 2 cells that drive lung inflammation. J Exp Med. 2003; 198:315–24. [PubMed: 12860930]
46. Teng MW, Swann JB, Koebel CM, Schreiber RD, Smyth MJ. Immune-mediated dormancy: an equilibrium with cancer. J Leukoc Biol. 2008; 84:988–93. [PubMed: 18515327]

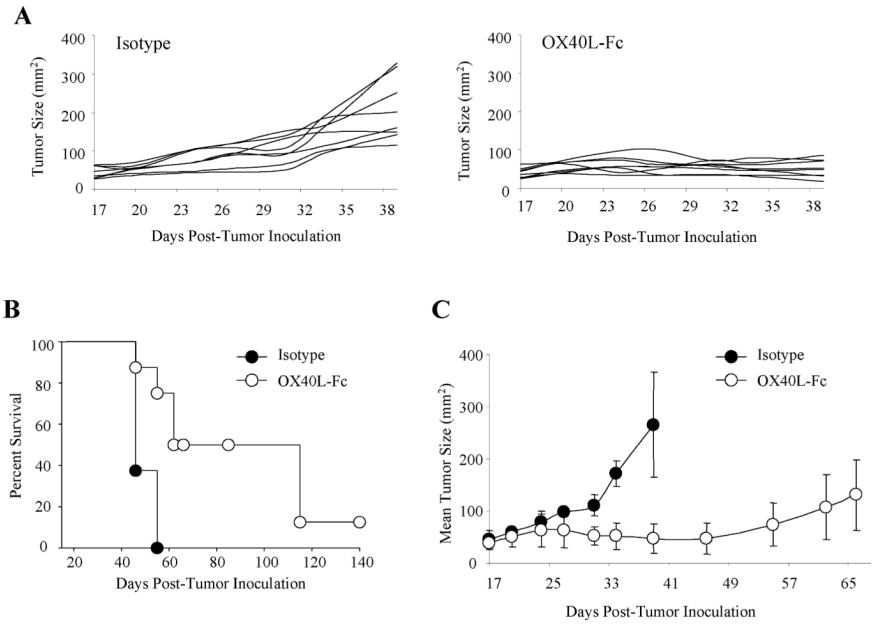

Figure 1. Systemic OX40L-Fc treatment is therapeutic against well-established tumors in wild-type mice

(**A**) MCA205 sarcomas (*n* = 8 per group) were injected s.c. into the right flank of C57BL/6 wild-type mice. Mice bearing established day 17 tumors (~30 to 50 mm^2 in area) were treated i.p. with 100 μg of rat IgG isotype control mAb or OX40L-Fc, as indicated. Treatment was repeated on day 20 after tumor inoculation. Tumor areas (mm^2) were calculated every 3 days, with the data for individual animals reported. (**B**) Data from **Fig. 1A** are presented in a Kaplan-Meier plot. (**C**) Mean tumor areas ± SD are shown for representative OX40L-Fc-treated mice exhibiting tumor dormancy (*n* = 3), with data obtained from isotype-treated control animals (*n* = 3) shown for comparison. Data are representative of two independent experiments performed.

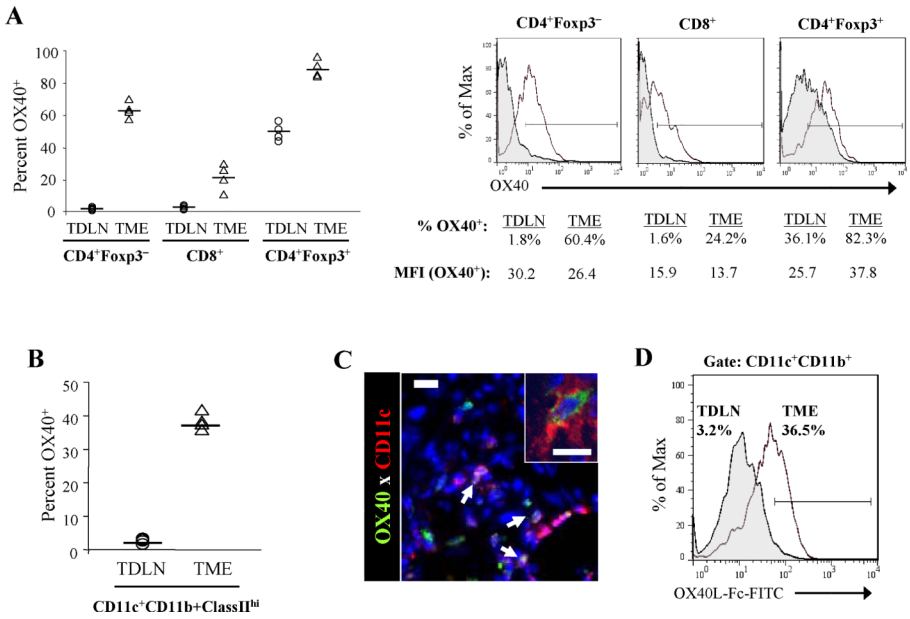

Figure 2. T cell and DC expression of OX40 is elevated in the progressive TME in wild-type mice

(**A** and **B**) Single-cell suspensions (n = 4) were prepared from untreated MCA205 tumors (TME) and tumor-draining lymph nodes (TDLN) isolated between days 17 and 20 post-tumor inoculation. (**A**) Percentages of $OX40^+$ T cells among the indicated gated cell populations are shown (left panel). Each symbol corresponds to an individual tumor-bearing mouse (bar = median value). Representative histograms are depicted (right panel), with percentages of $OX40^+$ T cells and mean fluorescence intensity (MFI) of $OX40^+$ T cells indicated. Filled histograms represent cells isolated from the TDLN; open histograms represent cells isolated from the TME. (**B**) Percentages of DC ($CD11c^+CD11b^+ClassII^{hi}$) expressing OX40 in the TDLN and TME are reported (bar = median value). (**C**) Untreated MCA205 tumors were isolated between days 17 and 20 post-tumor inoculation, then sectioned, stained and analyzed by confocal fluorescence microscopy as described in Materials and Methods. Representative staining of DAPI (blue), OX40 (green) and CD11c (red) is shown, with arrows indicating $CD11c^+OX40^+$ cells. Inset reflects higher power (60× magnification) image. Bars, 10 μm. (D) Representative staining of gated $CD11c^+CD11b^+$ DC with FITC-labeled OX40L-Fc. Filled histogram represents cells isolated from the TDLN; open histogram represents cells isolated from the TME. Experiments were repeated two times with similar results obtained in each instance.

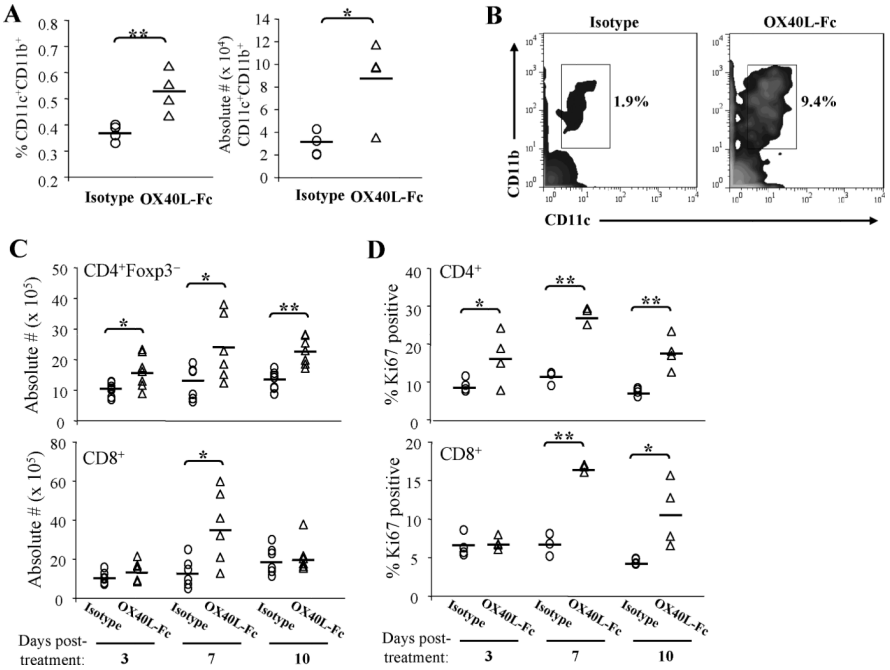

Figure 3. Longitudinal analysis of TDLN populations following OX40L-Fc treatment

MCA205 tumor-bearing wild-type or $Rag^{-/-}$ mice were treated as in Fig. 1 and TDLN cells were isolated on day 3 after treatment with isotype control antibody or OX40L-Fc ($n = 4$ per group). In **A**, the percentages and absolute numbers ($\times 10^4$) of $CD11c^+CD11b^+$ DC among gated live cells are shown for wild-type mice. Each symbol corresponds to an individual animal. The solid line represents the median value. In **B**, a representative density plot is shown, with percentages indicated for $CD11c^+CD11b^+$ DC among total TDLN cells isolated from $Rag^{-/-}$ mice. For panels **C** and **D**, TDLN cells were isolated from wild-type mice on days 3, 7, and 10 after treatment. Graphs show absolute numbers ($\times 10^5$) of $CD4^+Foxp3^-$ and $CD8^+$ T cells (**C**) and the percentages of $Ki67^+$ T cells (**D**). Data are representative of results obtained in 2 independent experiments in each case. *, $P < 0.05$; **, $P < 0.01$.

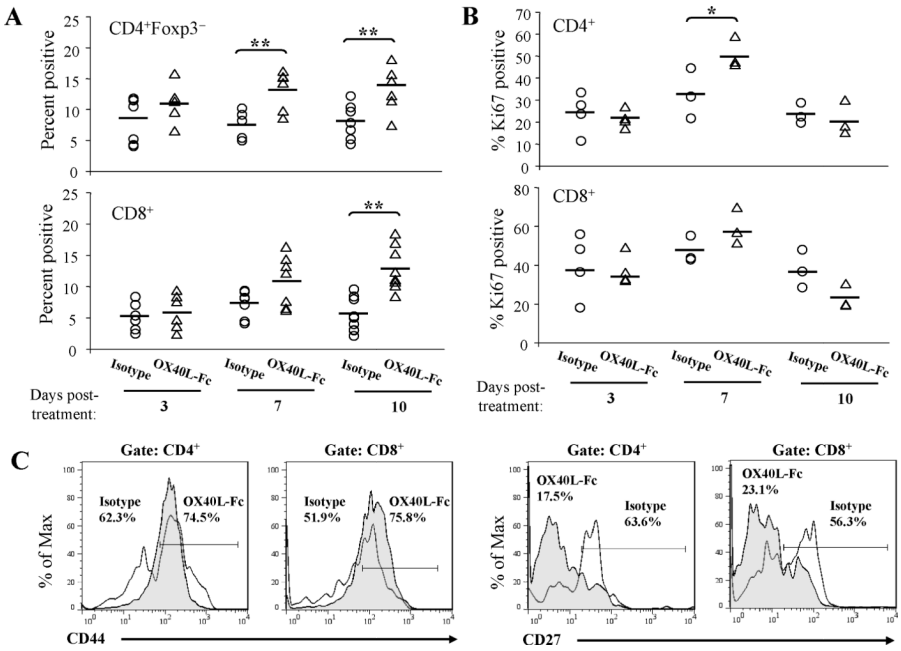

Figure 4. Accumulation of T effector cells in the TME of wild-type mice by day 10 following OX40L-Fc treatment

TME cells were isolated on days 3, 7, and 10 after treatment with isotype control antibody or OX40L-Fc. Graphs show percentages of $CD4^+Foxp3^-$ and $CD8^+$ T cells (**A**) and percentages of $Ki67^+$ T cells (**B**). Each symbol corresponds to one tumor-bearing mouse. The solid line represents the median value. (**C**) TIL were isolated on day 10 after treatment with isotype control antibody or OX40L-Fc. Percentages of $CD44^{hi}$ of $CD4^+$ and $CD44^{hi}$ of $CD8^+$ cells are indicated on representative histograms. CD27 was evaluated on gated $CD4^+$ and $CD8^+$ cells, as indicated (representative histograms are shown). Open histograms represent cells isolated from isotype control mAb-treated mice; filled histograms represent cells isolated from OX40L-Fc-treated mice. Similar data were obtained in two independent experiments performed. *, $P < 0.05$; **, $P < 0.01$.

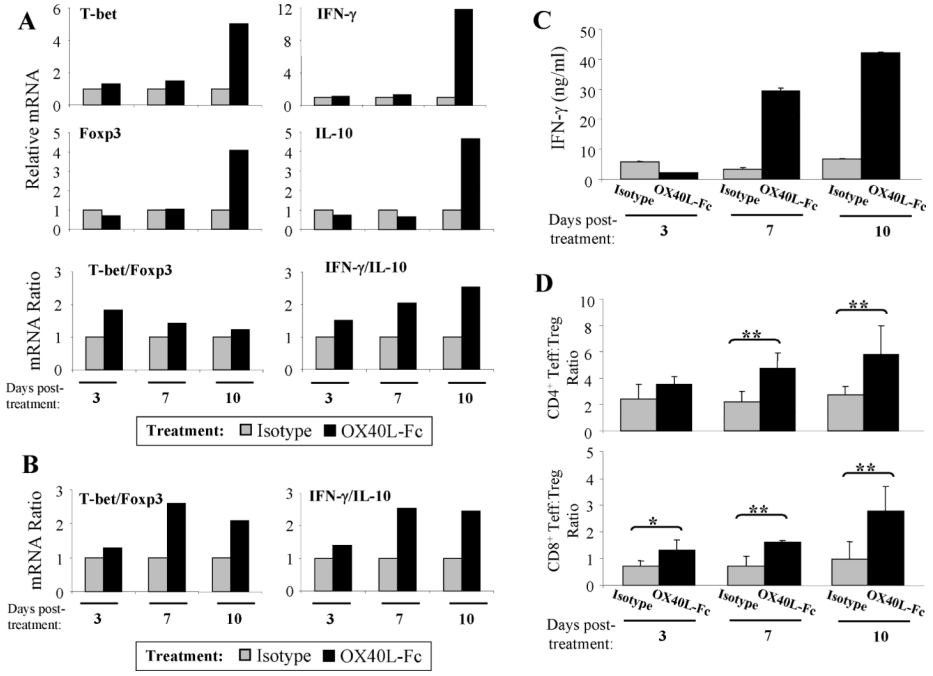

Figure 5. TIL exhibit a Type-1 polarized phenotype

TIL were isolated from wild-type mice on days 3, 7, and 10 after treatment with isotype control antibody or OX40L-Fc. (**A**) Quantitative RT-PCR was performed on purified RNA (*n* = 2 per group, pooled) using primers specific for murine T-bet, Foxp3, IFN-γ, and IL-10. ΔΔCt were calculated to day 3 isotype treatment samples and relative RNA expression for each gene is depicted as $2^{\Delta\Delta Ct}$ (upper panels). Ratios of T-bet/Foxp3 and IFN-γ/IL-10 are also shown (lower panels). Similar data were obtained in two independent experiments performed. (**B**) TIL were stimulated with anti-CD3 for 24 hours *in vitro* as outlined in Materials and Methods, with semi-quantitative RT-PCR performed on purified RNA (*n* = 2 per group, pooled) using primers specific for murine T-bet, Foxp3, IFN-γ, and IL-10. Similar data were obtained in two independent experiments performed. (**C**) Isolated TIL were re-stimulated *in vitro* with irradiated MCA205 cells for five days (as described in Materials and Methods). Recovered T cells were then stimulated with anti-CD3 for 72 hours and supernatants were assessed for levels of IFN-γ. Data are reported as the mean ± SD of duplicate determinations. Similar data were obtained in two independent experiments performed. (**D**) $CD4^+Foxp3^-$ and $CD8^+$ T effector-to-$CD4^+Foxp3^+$ Treg cell ratios were determined by flow cytometry (*n* = 4 per group). Data are representative of three independent experiments performed. *, $P < 0.05$; **, $P < 0.01$.

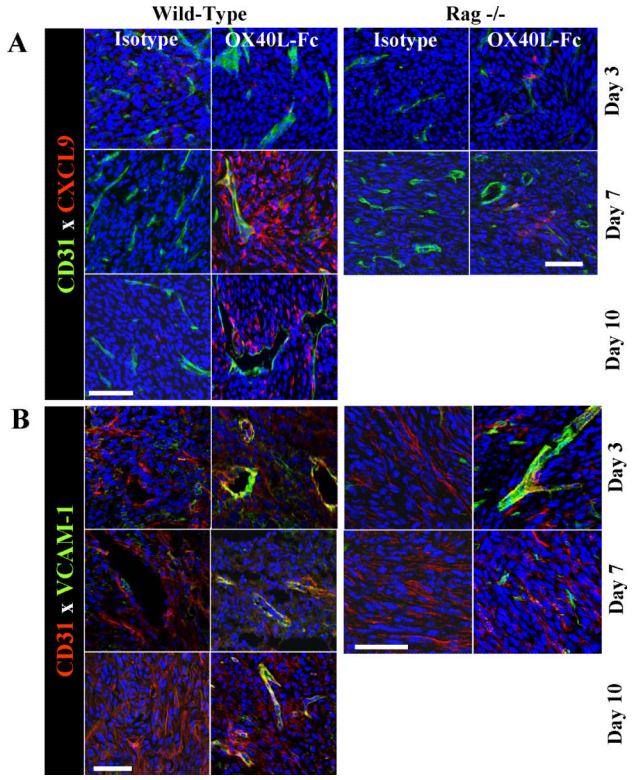

Figure 6. T cell-independent up-regulation of VEC-associated CXCL9 and VCAM-1 in the TME following OX40L-Fc treatment

MCA205 tumors were isolated from wild-type (left panels) or $Rag^{-/-}$ (right panels) mice and analyzed by confocal fluorescence microscopy on the indicated days after treatment with isotype control antibody or OX40L-Fc. In **A**, expression of DAPI (blue), CXCL9/Mig (red), and CD31 (green) is depicted. In **B**, expression of DAPI (blue), CD31 (red) and VCAM-1 (green) is depicted. Bars, 50 μm.